Applied Geochemistry 191 (2025) 106516

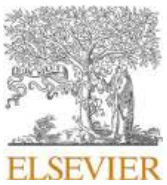

Contents lists available at ScienceDirect

Applied Geochemistry

journal homepage: www.elsevier.com/locate/apgeochem

Fumarolic CO_2 emissions from weakly degassing, hydrothermal volcanoes: a case from Fogo volcano, São Miguel, Azores

Alessandro Aiuppa [a,*], Fátima Viveiros [b,c], António Cordeiro [b,d]

[a] Dipartimento DiSTeM, Università di Palermo, Palermo, Italy
[b] Instituto de Investigação em Vulcanologia e Avaliação de Riscos (IVAR), Universidade dos Açores, Ponta Delgada, Açores, Portugal
[c] Faculdade de Ciências e Tecnologia, Universidade dos Açores, Ponta Delgada, Açores, Portugal
[d] Centro de Informação e Vigilância Sismovulcânica dos Açores (CIVISA), Ponta Delgada, Açores, Portugal

ARTICLE INFO

Editorial handling by: Elisa Sacchi

Keywords:
CO_2 fluxes
Hydrothermal systems
Fogo volcano
Volcanic gases

ABSTRACT

Current global catalogues of hydrothermal CO_2 emissions from quiescent volcanoes are manifestly incomplete, primarily because of the shortage of available flux measurements. Fogo, a quiescent stratovolcano volcano in the central part of São Miguel island (Azores, North Atlantic Ocean), is an emblematic example of such hydrothermal systems that lack assessment of fumarolic gas fluxes. Here, for the first time, we characterize the CO_2 flux emissions from the main hydrothermal manifestations (steaming grounds, boiling pools and fumaroles) of this volcano. For this, we use the results of a ground-based CO_2 profiling campaign, carried out using a portable Multi-GAS unit. We find these hydrothermal manifestations to be very CO_2-rich and H_2S–H_2-poor, with CO_2/H_2S and H_2/CO_2 ratios of respectively 1600–80,700 and $2{\cdot}10^{-4}$ to $2{\cdot}10^{-3}$. We additionally show that these emissions, although very modest at visual observation, still emit CO_2 at levels of 1.3 to 95 tons/day, for a cumulative fumarolic CO_2 flux of 232 ± 140 tons/day for the volcano. This is ~6 times higher than the CO_2 flux from diffuse soil degassing in the Caldeiras da Ribeira Grande area, and of the same order of the CO_2 flux sustained by crater plume degassing at a typical medium-sized arc volcano. The contribution of weak hydrothermal manifestations (steaming grounds, boiling pools and fumaroles) to the global volcanic CO_2 budget is undetermined, but may have been overlooked so far.

1. Introduction

Carbon dioxide (CO_2) is the second most abundant volatile in magmas (Wallace et al., 2015), and in the volcanic gases they emit by degassing (Oppenheimer et al., 2014). The central role played by volcanic CO_2 emissions on pre-industrial atmospheric CO_2 levels (Steinthorsdottir et al., 2025), and hence on climate evolution over geological timescales (Sleep and Zahnle, 2001), have motivated efforts to assess how much CO_2 is released by subaerial volcanism globally (Gerlach, 1991). It has long been accepted that the volcanic CO_2 budget from subaerial volcanism is primarily sustained by a relatively small number of large volcanic point sources (Williams et al., 1992). However, recent progress achieved in the context of the Deep Carbon Observatory (DCO) initiative (https://deepcarbon.science/) has partially revised this view (Fischer and Aiuppa, 2020). It is now believed that, in addition to the strong volcanic gas emitters (Aiuppa et al., 2019), a large fraction of the CO_2 budget is potentially contributed by less visible forms of degassing, such as volcanic lakes (Pérez et al., 2011), soils from volcanoes and nearby tectonically active regions (Burton et al., 2013; Fischer et al., 2019; Werner et al., 2019; Wong et al., 2019), and weak fumaroles/steaming grounds from dormant/hydrothermal volcanoes (Fischer et al., 2019). This latter form of degassing is the subject of the present work.

It is estimated (Fischer et al., 2019) that roughly one third of the ~900 Holocene volcanoes, registered in global volcano catalogues (Syracuse and Abers, 2006; Global Volcanism Program, 2024), today exhibit weak hydrothermal degassing activity from low-temperature fumaroles, steaming grounds, and bubbling pools. These emissions contain no, or little SO_2, hence cannot be quantified (for flux) by conventional UV spectroscopy (Oppenheimer et al., 2014). Yet the sparse results available (Fischer et al., 2019; Fischer and Aiuppa, 2020) suggest these hydrothermal volcanoes may daily release tens of tons of CO_2 each, for a potential cumulative yearly CO_2 output of 3–4 Tg. As this cumulative flux is derived from extrapolation from the very limited

* Corresponding author.
E-mail address: alessandro.aiuppa@unipa.it (A. Aiuppa).

https://doi.org/10.1016/j.apgeochem.2025.106516
Received 14 May 2025; Received in revised form 23 July 2025; Accepted 2 August 2025
Available online 7 August 2025

existent data, and is hence subject to severe uncertainties, there is an urgent need for more observations and data acquisition.

One volcano exhibiting this degassing activity style is Fogo (also referred as Vulcão de Água de Pau). This relatively large (area, 132 km^2; elevation, 947 m) stratovolcano (Fig. 1a and b) occupies the central region of São Miguel island, in the Azores (North Atlantic Ocean; Fig. 1c), and has been recurrently active in the last 10 ka, including two trachytic Plinian eruptions dated at 8–12 and 4.6 ka BP (Walker and Croasdale, 1971; Wallenstein et al., 2015). This volcano has been dormant since the last two historical eruptions in 1563–1564 CE (Moore, 1990; Wallenstein et al., 2015) and it is today topped by a summit caldera filled by a cold lake (Lagoa do Fogo) (Fig. 1b) (Andrade et al., 2020). Current signs of activity include the recurrent seismic swarms (Silva et al., 2012, 2020), episodes of ground deformation (D'Araújo et al., 2022), and a variety of surface hydrothermal manifestations, concentrating essentially on the northern flank of the volcano (Fig. 1c) mainly associated with the NW-SE-trending Ribeira Grande Graben (Caliro et al., 2015; Viveiros et al., 2015a, 2023). These manifestations

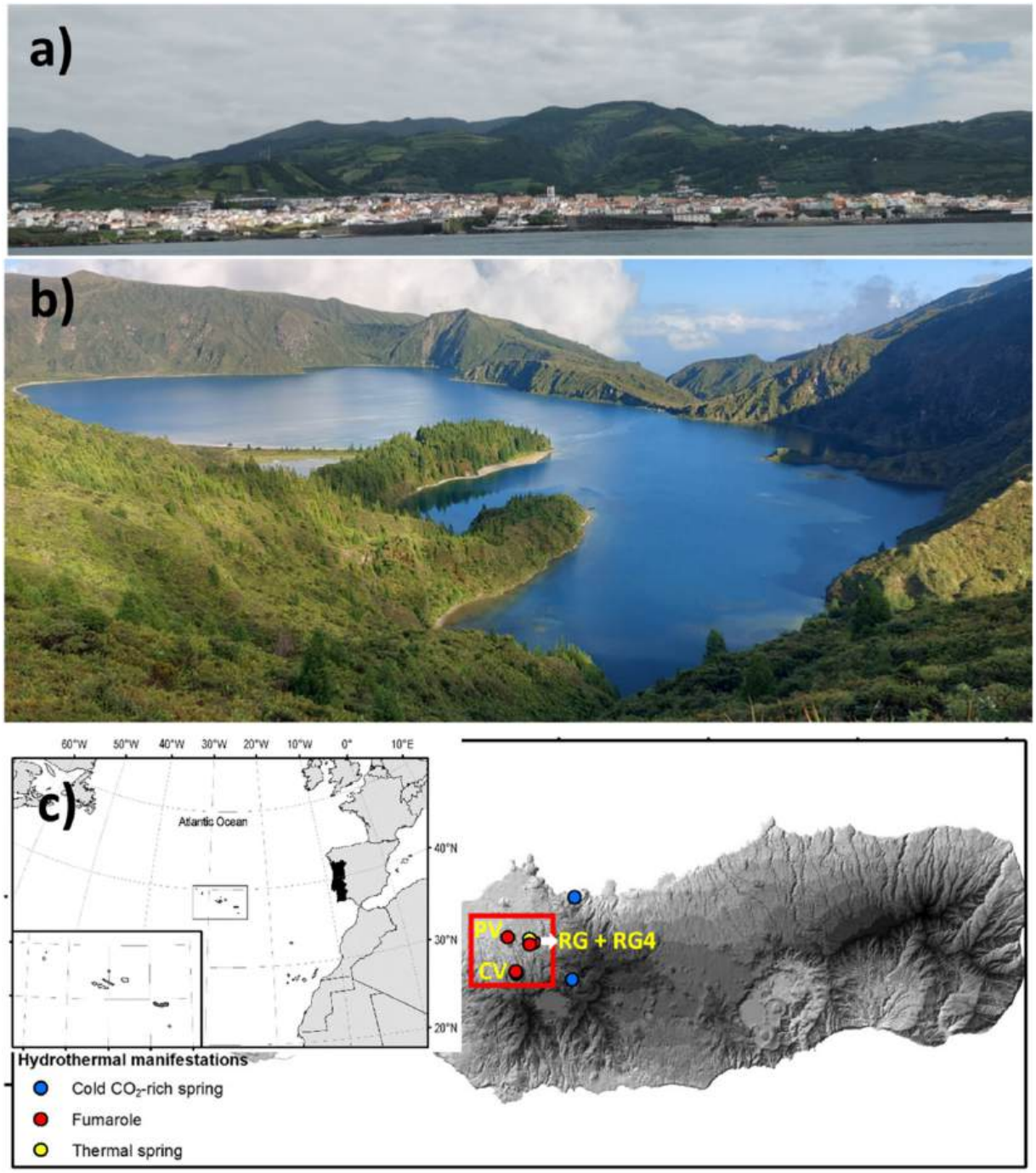

Fig. 1. a) Fogo volcano (also known as Água de Pau). Picture of the southern flank taken from the sea. b) Fogo caldera with its crater lake. c) DEM from the eastern side of São Miguel Island. The red square identifies the northern flank of Fogo volcano and corresponds to the area shown in Fig. 3. Location of the main hydrothermal manifestations at Fogo volcano. Yellow letters identify the fumarolic ground at Fogo volcano: PV – Pico Vermelho, CV – Caldeira Velha (and includes CVF and CVS), and RG + RG4 – Caldeiras da Ribeira Grande + Ribeira Grande 4 (comprise RGF, RGP, RG4, and RG4L). Figure insect with the location of the Azores archipelago in the Atlantic Ocean. São Miguel Island is black shadowed. (For interpretation of the references to color in this figure legend, the reader is referred to the Web version of this article.)

are interpreted as the surface expression of a large geothermal system (reservoir temperature, ~256 °C), exploited by several geothermal wells in the so-called "Ribeira Grande geothermal field" (Carvalho et al., 2006; Pereira et al., 2022). Fumaroles and steaming grounds exhibit hydrothermal compositions and maximum temperatures of ~99 °C (Caliro et al., 2015; Pereira et al., 2022; Matias et al., 2024). Soil emissions are dominated by CO_2 and concentrate on the volcano's northern flank. However, recent work has also identified a diffuse degassing structure in the southern flank of the volcano (Pimentel, 2024). CO_2 soil fluxes in the Caldeiras da Ribeira Grande area - and their potential public health implications - have thoroughly been investigated by Viveiros et al. (2008, 2015a, b), and a daily output of ~40 (±1.4) tons CO_2 has recently been estimated for the area by Viveiros et al. (2023). In contrast, no similar information exists for the fumarolic CO_2 output, although numerical simulations (Viveiros et al., 2023) suggest this may be in the order of ~174 tons/day. Quantifying this fumarolic CO_2 flux is the purpose of this study.

2. Methodology

At mildly degassing hydrothermal volcanoes, measurements of the fumarolic CO_2 emission rates is challenged by the absence of SO_2 in these emissions (Aiuppa et al., 2017; Stix and de Moor, 2018), preventing from use of spectroscopic techniques that use the interaction of

Fig. 2. Fogo volcano main hydrothermal manifestations. a) Caldeiras da Ribeira Grande Fumarole (RGF), b) Pico Vermelho steaming ground (PV), c) Caldeiras da Ribeira Grande boiling pool (RGP), d) Ribeira Grande 4 Levadas (RG4L), e) Caldeira Velha Fumarole (CVF), f) Ribeira Grande 4 steaming ground (RG4).

this gas with sunlight in the UV region (Oppenheimer et al., 2011). To quantify the CO_2 flux, one must then rely on profiling CO_2 concentrations over a cross-section of the fumarole's atmospheric plume that, by integration over the whole plume cross-sectional area, and after multiplication by the plume's transport speed, can then yield a flux. For relatively large emitters, this procedure can be realized by airborne plume CO_2 profiling via either fixed-wing aircrafts (Werner et al., 2009) or Unmanned Aircraft Systems (UAS; James et al., 2020). However, for small emissions, near-vent ground-based measurements remain the only viable option.

In this study, we quantify the fumarolic CO_2 flux from the six most visible natural hydrothermal manifestations of the Fogo volcano (Fig. 2) following a methodology developed for Campi Flegrei volcano by Aiuppa et al. (2013). The locations of the target manifestations are shown in Figs. 1c and 3a. As shown by Fig. 2, these manifestations take a variety of forms, including steaming grounds (RG4 main area - RG4, RG4 Levadas - RG4L), bubbling pools (Caldeiras da Ribeira Grande pool – RGP), boiling temperature fumarolic fields (Pico Vermelho - PV), and boiling temperature fumaroles with adjacent boiling pools (Caldeiras da Ribeira Grande Fumarole - RGF and Caldeira Velha Fumarole - CVF). Caldeira Velha and Caldeiras da Ribeira Grande fumaroles show, respectively, areas of 164 and 69 m^2 (totaling 277 m^2 with the adjacent boiling pools). These emissions consist mainly of water vapor with CO_2 as the main gas in the dry phase, followed by H_2S. Caldeira Velha's emissions are richer in CH_4 compared to the Caldeiras da Ribeira Grande (Pereira et al., 2022; Matias et al., 2024). Equilibrium temperatures for the reservoirs feeding these fumaroles have been recently defined by Matias et al. (2024) and are higher at Caldeiras da Ribeira Grande

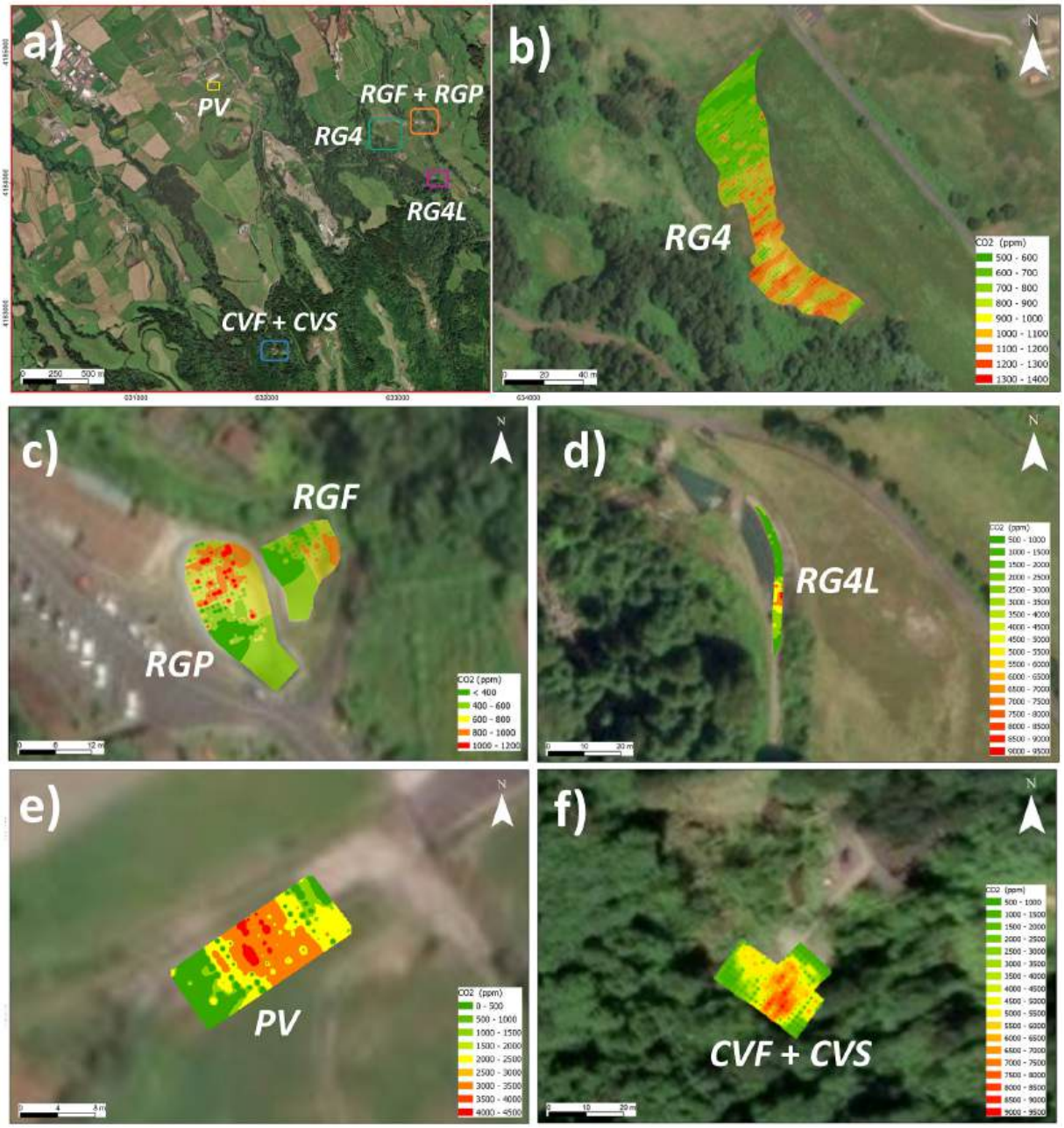

Fig. 3. – a) Location of the study sites. E-type CO_2 concentration maps for b) RG4 - Ribeira Grande 4, c) RGF - Caldeiras da Ribeira Grande Fumarole and RGP - Caldeiras da Ribeira Grande Pool, d) RG4L - Ribeira Grande 4 Levadas, e) PV - Pico Vermelho fumaroles, f) CVF - Caldeira Velha Fumarole + CVS – Caldeira Velha small.

(240–262 °C) than at Caldeira Velha (223–232 °C). Caldeiras da Ribeira Grande's pool consists of an artificial tank where thermal fluids mix with rainwater. The maximum temperature measured by Carvalho et al. (2006) was 49 °C, and the pH varied between 2.66 and 5.53. CO_2 is the main dissolved volatile in these waters (136–482 mg/L). The steaming ground (RG4 main area and Levadas) appeared after 2010 due to the drilling of a geothermal well and show maximum soil temperatures of around 100 °C (Uchôa et al., 2023), with the main released gases being water vapor and CO_2 (Viveiros et al., 2023). Caliro et al. (2015) analyzed the gases released in the RG4 main area and the equilibrium temperature obtained for the feeding reservoir was the highest of all the emissions at Fogo volcano (272–278 °C). Pico Vermelho emissions are essentially water vapor with minor amounts of CO_2. According to Pereira et al. (2022), the N_2/O_2 ratio in these emissions reflects air addition in the subsurface.

In each of these manifestations, we estimate the CO_2 flux using a methodology (Aiuppa et al., 2013) that involves use of a portable Multi-GAS unit (same configuration as in Aiuppa et al., 2022) to measure (by near-dispersive infra-red spectroscopy; sensor model NG Gascard from Edinburgh Sensors, calibration range, 0–300,000 ppm) the spatial distribution of CO_2 concentrations over a horizontal cross-section of the fumarole/pool/steaming ground atmospheric plume (Fig. 3). For this, during field operations, two operators are positioned on opposite sides of the manifestation (Fig. 2a and b), with a graduated rope held by them that is used to manually and sequentially scroll the Multi-GAS inlet from one end to the other, while the Multi-GAS is recording concentrations every second. A ~10 m long silicone tubing is attached to the rope and serves as the inlet for the Multi-GAS (the same tubing/rope system was used at all sites). The use of this long inlet system was tested and verified at Campi Flegrei, providing an excellent correlation between fumarole (from direct sampling) and plume (Multi-GAS) compositions, at least for the CO_2/H_2S and CO_2/H_2 ratios. Operations were synchronized (with a chronometer) so as to have the Multi-GAS inlet sequentially stopped at nodes 1 m apart, where CO_2 concentrations were measured at a 1 Hz rate for 20 s, before moving to the next node. Doing so, and with successive repositioning of the operators (see Aiuppa et al., 2013), CO_2 concentration results were obtained along a regular horizontal grid with node spacing of 1 m × 1 m (note that the 20 concentration measurements at each node are averaged during post-processing). Depending on the size of the manifestation, a full grid, covering the entire plume cross-section, is completed in ~30–~120 min. Where possible, each manifestation is profiled twice to test repeatability (see below). Care is taken to conduct these measurements during calm wind conditions, to ensure the reconstructed horizontal cross-section is roughly perpendicular to the vertically rising atmospheric plume (Fig. 2). Concurrently with the Multi-GAS profiling procedure described above, a video camera (GoPro Hero 2) was used to record (at 25–100 frames/s) a sequence of images of the atmospheric plume itself.

During post-processing, the Multi-GAS dataset is treated by initially subtracting the atmospheric background CO_2 concentrations (420 ppmv, from background measurements upwind from the hydrothermal areas). Then, the background corrected CO_2 concentrations are interpolated using the sequential Gaussian simulation methodology (Deutsch and Journel, 1998). The variograms used for each site, to produce the 100 simulations, are shown as Supplementary Materials (Supplementary Fig. 1). The resulting e-type maps, i.e., the mean maps from the 100 simulations (Deutsch and Journel, 1998), are shown in the maps of Fig. 3. A 2D integration over the entire cross-sectional area returns the CO_2 Integrated Column Amounts (ICAs) for each manifestation, listed in Table 1. These are then converted into fluxes by multiplying by plume's transport speed, which is estimated by manually processing (using the ImageJ software; https://imagej.net/ij/index.html) the sequences of images collected by the video camera. Here, transport speed is quantified by manually tracking the movement of individual gas puffs (a graduated pole is used to convert camera pixel dimensions in the images

Table 1
Summary of observations. For each measurement site, we report the CO_2 integrated column amounts (ICA), expressed in both ppm·m^2 and kg/m (we use the in-situ measured plume temperature and atmospheric pressure for the conversion). The CO_2 flux is calculated by multiplying ICA by plume speed. The relative molar abundances of other gases (normalized to CO_2) in the plume are also shown. The H_2S and H_2 fluxes are derived by multiplying the CO_2 flux by the plume H_2S/CO_2 and H_2/CO_2 ratios. Uncertainty is expressed at 1 standard deviation (SD).

Site	CO_2 ICA (ppm m^2)	SD	CO_2 ICA (kg/m)	Plume speed (m/s)	SD	CO_2 flux (kg/s)	SD	CO_2 Flux (tons/day)	SD	H_2O/CO_2	CO_2/H_2S	H_2S/CO_2	SD	CO_2/H_2	H_2/CO_2	SD	H_2S flux (tons/day)	H_2 flux (tons/day)
Ribeira Grande 4 (RG4)	2070931	352058	3.6	0.3	0.1	1.0	0.5	87	46	6.7	80742	1.2E-05	4.1E-06	4654	0.000215	6.2E-05	0.001	0.0009
Ribeira Grande 4 Levadas (RG4L)	178537	30351	0.3	0.8	0.2	0.25	0.1	22	9	17	8422	0.00012	1.4E-05	709	0.00141	0.00031	0.002	0.0014
Caldeiras da Ribeira Grande Fumarole (RGF)	14123	2401	0.025	0.6	0.1	0.02	0.01	1.3	0	9.5	1700	0.00059	8.7E-05	557	0.001795	0.00027	0.001	0.0001
Caldeiras da Ribeira Grande pool (RGP)	97900	16643	0.17	0.5	0.1	0.09	0.03	8	3	10	1500	0.00067	0.00038	406	0.002463	0.00070	0.004	0.0009
Pico Vermelho (PV)	55089	9365	0.098	1.1	3	0.1	0.3	9	27	7.0	9596	0.00010	3.1E-05	1427	0.000701	8.3E-05	0.001	0.0003
Caldeira Velha Fumarole (CVF)	167756	28518	0.298	3.7	1.3	1.1	0.6	95	50	0.5	2803	0.00036	1.5E-05	948	0.001055	5.4E-05	0.028	0.0046
Caldeira Velha small (CVS)	15686	2667	0.028	3.7	1.3	0.1	0.05	9	5	2.5	1609	0.00062	6.0E-05	1269	0.000788	0.00015	0.005	0.0003
TOTAL FLUX						**2.7**	1.6	**232**	140								**0.04**	**0.0084**

into real distance, and the vertical component of the transport speed is calculated in all cases). The geometry of these individual buoyant, vertically rising puffs is easy to resolve and track, as the plume is condensing (and hence optically visible) during atmospheric transport (Fig. 2).

Uncertainty in the derived CO_2 fluxes reflects propagation of errors in (i) CO_2 concentrations, (ii) profiling operations (iii) data processing, and (iv) plume transport speed calculation. Laboratory tests with standard gas mixtures indicate that at the concentration levels measured in the current area (typically several hundreds to thousands of ppmv above atmospheric background, Fig. 3), uncertainty in individual CO_2 concentrations is $\leq$ 5 %. This standard error level is confirmed by standard deviations of measurements on the individual node points, which are typically $\leq$5 %. Errors during field (profiling) and post-field (processing) operations are more difficult to quantify, as they can arise from a variety of causes (for example, incorrect positioning of the measurement nodes, incomplete coverage of the entire plume cross-sectional area, errors in the statistical analysis used for data interpolation). However, we can indirectly estimate a ~17 % uncertainty from comparison of ICAs derived in replicated profiles obtained at some target manifestations (Table 1 and Aiuppa et al., 2013). Finally, we take the standard deviation of the derived transport speeds (~26 % on average) to quantify the total uncertainty in the derived fluxes at $\leq$48 %.

In addition to CO_2, the Multi-GAS is configured to measure the concentrations of other gas species, including SO_2 (CiTiceL electrochemical sensor model T3STF), H_2S (CiTiceL electrochemical sensor model T3H) and H_2 (CiTiceL electrochemical sensor model T3HYT). All sensors were calibrated (in the 0–200 ppm calibration range) in the laboratory prior to and after field work using certified standard gases. A KVM3/5 Galltec-Mela sensor was also used for measuring temperature and relative humidity and to indirectly estimate H_2O concentrations in the plume using the Arden-Buck equation (Buck, 1981). At the field conditions encountered, the plume is always condensing (relative humidity >90 %), rendering water condensation in the inlet (tubing) system very likely. Hence, the derived H_2O results underestimate the real fumarolic H_2O/CO_2 ratios. SO_2 is undetectable in all the six

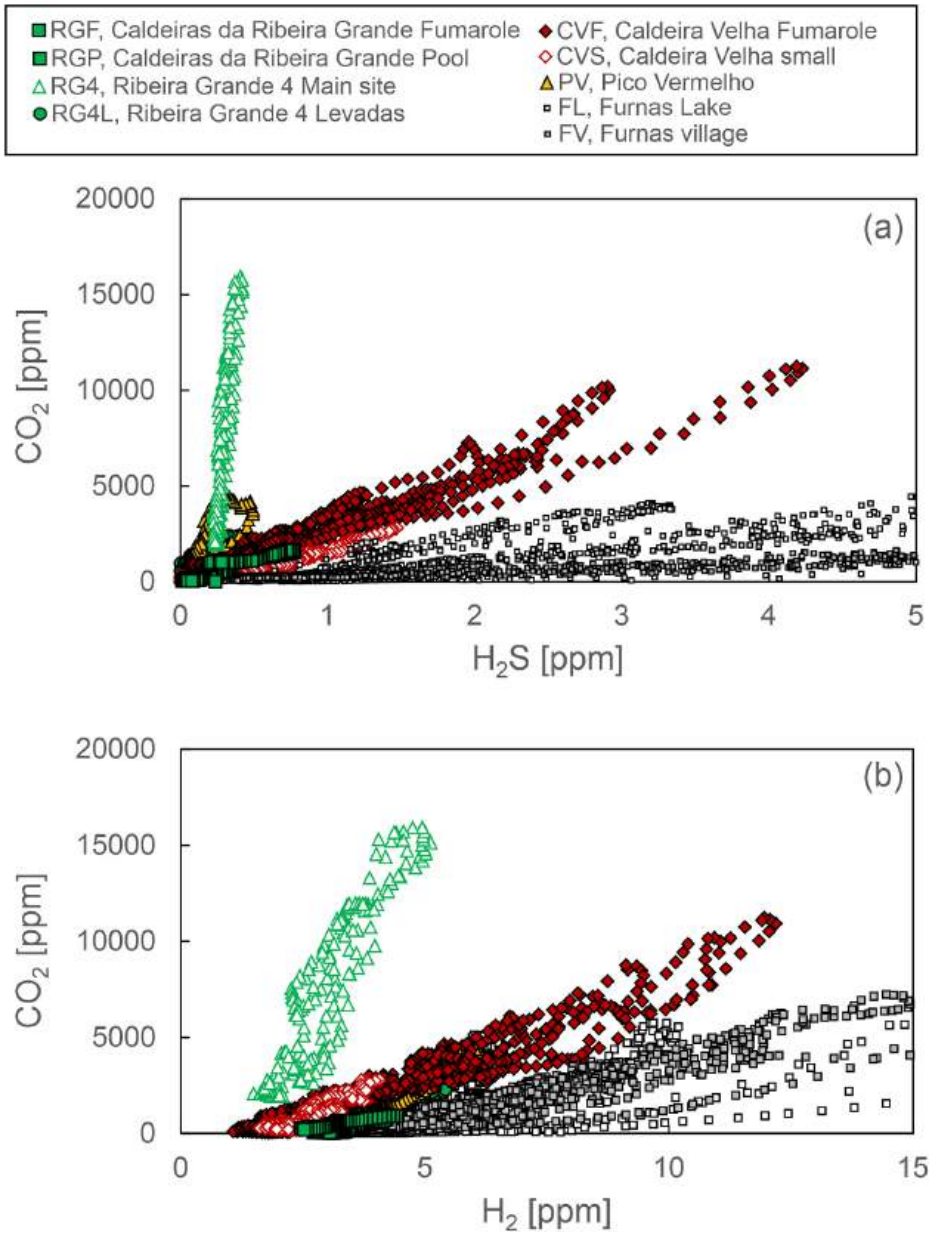

Fig. 4. – Scatter plot of (a) CO_2 vs H_2S and (b) CO_2 vs H_2 concentrations, as measured in the atmospheric plumes of the Fogo volcano hydrothermal manifestations, as measured by the Multi-GAS. For comparison, similar composition results acquired at the Furnas hydrothermal site (east São Miguel island) are also shown.

manifestations studies, consistent with their hydrothermal nature. H_2S and H_2 are detected at all sites, and their concentrations exhibit strong positive correlations with CO_2 concentrations (Fig. 4). The H_2S/CO_2 and H_2/CO_2 ratios are hence inferred from the slopes of the best-fit regression lines, and hence multiplied by the estimated CO_2 fluxes to convert into H_2S and H_2 fluxes (Table 1).

3. Results

Fig. 3 illustrates the contour maps of CO_2 concentrations at the studied manifestations, obtained after interpolation of field measured, background-corrected CO_2 concentrations using the sequential Gaussian simulation methodology (Deutsch and Journel, 1998). These maps convey information on the location of the most actively degassing spots (peaks in CO_2 concentrations), and on the in-plume concentration diversity. Broadly speaking, all maps contain a central core of high CO_2 concentrations that spatially correspond to the most actively degassing areas, surrounded by areas with close-to-background concentrations at the margin of each manifestation. In the maps' cores, CO_2 concentrations are typically several thousand ppm above background, with maxima (9000–9500 ppm CO_2) observed at CVF and RG4L (Fig. 3). At the margins, CO_2 concentrations remain tens to a few hundred ppm above background. Even if the sampling strategy is the same in the various study sites, variogram models and parameters are different (Fig. S1 – Supplemental Material). These differences reflect the variety of field conditions encountered, such as the dimension and shape of the study site, permeability of the soil, and distinct topography.

Integration over the entire plume cross-sectional area allows calculating the CO_2 ICAs listed in Table 1. By definition, the ICA is a combined indicator that takes into account both the extension (as parametrized by cross-sectional area) and vigor (as indicated by CO_2 concentrations peak levels and range) of each manifestation. For example, the largest ICA ($2.07 \cdot 10^6$ ppm$\cdot$m^2, or 3.6 kg/m at 30 °C temperature; this is the average temperature of the atmospheric plume) is obtained for RG4, the largest in size (although the weakest in terms of CO_2 concentrations) degassing area. The lowest ICA is obtained for site RGF ($1.4 \cdot 10^4$ ppm$\cdot$m^2, or 0.025 kg/m) (Table 1), reflecting its relatively small cross-sectional area and CO_2 concentration levels (Fig. 3).

The vertical component of the plume transport speed, as inferred from processing of video camera frames, ranges between 0.3 and 3.7 m/s at the different manifestations studied (Table 1). Correction for non-verticality of the plume was only required at PV. By multiplying plume transport speeds by the ICAs discussed above, we derive the CO_2 fluxes listed in Table 1. These range from 0.02 to 1.1 kg/s (1.3–95 tons/day). The total fumarolic CO_2 flux from Fogo volcano is hence 2.7 kg/s (232 ± 140 tons/day), and is dominated by two manifestations (RG4 and CVF) that contribute 79 % of the total budget.

In addition to CO_2, H_2S and H_2 are also detected in the atmospheric plumes of all the manifestations studied at ppm to sub-ppm levels (Fig. 4). The H_2S concentrations are the highest (from <0.1 to 4.2 ppm) at the Caldeira Velha sites (CVF and CVS). At the other sites, including those in the Ribeira Grande area, H_2S concentrations are systematically less than 1 ppm. For comparison, the atmospheric plumes of Furnas fumaroles (Furnas Lake - FL and Furnas Village - FV sites, two vigorously degassing hydrothermal sites located in the eastern part of São Miguel island; Ferreira and Oskarsson, 1999; Viveiros et al., 2010; Pedone et al., 2015) are more H_2S-rich, with peak in-plume concentrations of ~97 ppm (Fig. 4). The (molar) CO_2/H_2S ratios range from ~1600 (CVS) to ~80,700 (RG4) (equivalent to H_2S/CO_2 ratios of $6 \cdot 10^{-4}$ to $1.2 \cdot 10^{-5}$) (Table 1). For comparison, the Furnas sites have 1–2 orders of magnitude lower CO_2/H_2S ratios (of respectively 289 and 257 at FL and FV). The Caldeira Velha sites are also the richest in H_2, with a peak concentration of 12.2 ppm at CVF. At the Ribeira Grande sites, H_2 ranges between 1.8 and 5.3 ppm. The H_2/CO_2 ratios range from $2 \cdot 10^{-4}$ (RG4) to $2 \cdot 10^{-3}$ (RGF). The upper range is close to the range of variability observed at Furnas ($1.8–1.9 \cdot 10^{-3}$) (Table 1). We additionally report H_2O/CO_2 ratios for the atmospheric plumes of all manifestations. These range between 0.5 (CVF) to 17 (RG4L). Since the plumes were condensing at measurement conditions, we advise these ratios should be viewed as lower range estimates.

4. Discussion

The manifestations characterized in this study (Fig. 2) include steaming grounds, bubbling pools, and mildly degassing fumarolic fields (Fig. 2), and hence rank among the most inconspicuous forms of hydrothermal degassing encounterable at quiescent, hydrothermal volcanoes (Stix et al., 2025).

Compositionally, these manifestations are CO_2-enriched and sulphur-depleted relative to high-temperature magmatic gases (Fig. 5), as typical of low-temperature hydrothermal discharges formed by boiling of hydrothermal aquifers at depth (Chiodini and Marini, 1998). Comparison of our results with those of Caliro et al. (2015) and Pereira et al. (2022) (Fig. 5) indicates that the atmospheric plumes we studied are also compositionally more CO_2-rich and H_2S-poor than the fumaroles that immediately source them (directly sampled and characterized prior to atmospheric dilution by Caliro et al., 2015; Pereira et al., 2022). For example, the observed CO_2/H_2S ratios in the Caldeira Velha plumes are between ~1600 and 2800, while the directly sampled fumaroles (Caliro et al., 2015; Pereira et al., 2022) exhibit lower CO_2/H_2S ratios of ~400–600 (Fig. 5). Similarly, at Caldeiras da Ribeira Grande, the CO_2/H_2S ratios in plumes (1500–80,700; Table 1) are well higher than those measured in the fumaroles (179–3800; Caliro et al., 2015; Pereira et al., 2022). Plumes and source fumaroles also differ in terms of their H_2O/CO_2 ratios. According to the literature, the mean H_2O/CO_2 ratios in the fumaroles are 10.7 ± 2.9 (Caldeira Velha) and 14.3 ± 3.0 (Caldeiras da Ribeira Grande) (Caliro et al., 2015; Pereira et al., 2022), while our atmospheric plumes are considerably less H_2O-rich, especially at Caldeira Velha (H_2O/CO_2 ratios of 0.5–2.5). It is important to note that this plume vs. fumarole compositional contrast is not observed at Furnas (see Fig. 5), where fumaroles are far stronger in size and vigor. For example, the CO_2/H_2S ratios (257–289) obtained for the FL and FV plumes are within the range (127–449) reported in the literature based on direct fumarole sampling results (Caliro et al., 2015; Pedone et al., 2015 obtained a similar 150–353 range using the results of a Multi-GAS survey). Considering that Furnas results (Figs. 4–5) were obtained using the same instrument and during the same campaign, we can exclude that the plume/fumarole mismatch seen in the Fogo manifestations (Fig. 5) is caused by analytic artifacts (e.g., improper calibration/functioning of the Multi-GAS). In view of the above, we ascribe the mismatch between fumarole and plume compositions seen in Fig. 5 to a combination of (i) steam condensation in the Multi-GAS inlet system, mostly affecting H_2O, and being caused by the condensing nature of the plume studied and the relatively long tubing/inlet system used, and (ii) hydrothermal steam condensation in the near-surface (soil) and pool environments, also causing partial removal (scrubbing) of water-soluble H_2S, and hence leaving the residual gas (the atmospheric plume we sampled) relatively enriched in less water-soluble CO_2. This latter process is consistent with the presence of sulphur in the pools (as dissolved sulphate) and in the soil/sub-soils (where yellow-colored incrustations are common).

Despite their mild, apparently inconsistent nature, and very residual (in terms of extent of hydrothermal processing) compositional signatures, as discussed above, the Fogo hydrothermal manifestations do represent non-trivial sources of volcanic CO_2. We find that each of the manifestations emits CO_2 at tons per day level (range, 1.3–95 tons/day; Table 1). The cumulative fumarolic CO_2 flux from Fogo volcano is hence estimated at 232 ± 140 tons/day (Table 1). This is roughly equivalent to the typical CO_2 flux sustained by crater plume degassing at medium-sized, frequently active arc volcanoes worldwide, such as Asama (Japan), Kudryavy (Kamchatka) or Santa Ana (El Salvador) (see compilation of Werner et al., 2019). Hence, in analogy to what have been found for the even more "invisible" and "silent" diffuse soil

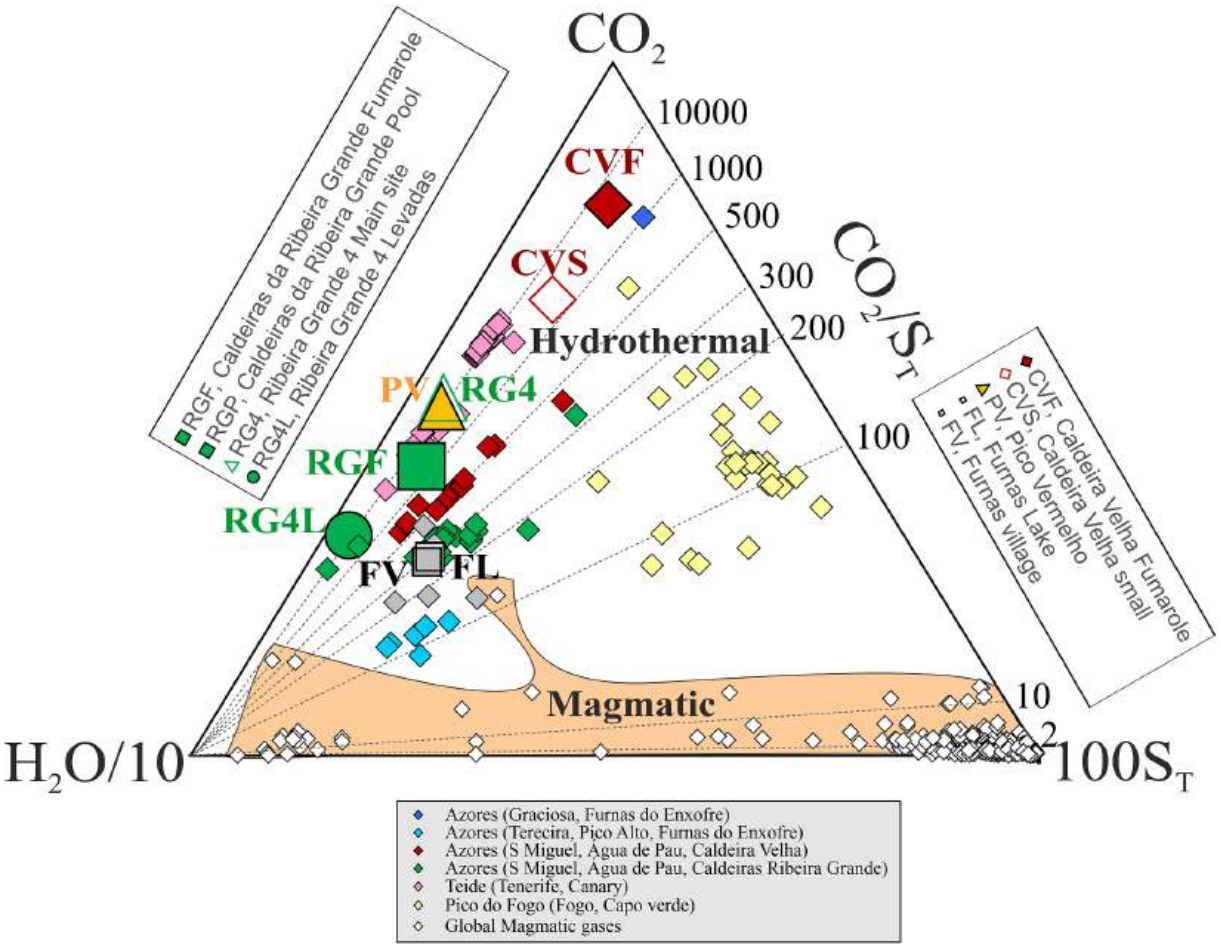

Fig. 5. Triangular plot illustrating the major element composition (in the COHS system) of the Fogo volcano fumaroles' atmospheric plumes (large symbols, this study). H_2O and total sulphur (S_T) are divided/multiplied by ad-hoc coefficients for illustration purposes. The Fogo fumarolic plumes plot on the CO_2-rich, S_T-poor end of the hydrothermal gas population, here indicated by: (i directly samples fumaroles from the same Fogo and other localities in the Azores (small diamonds; data from Caliro et al., 2015; Viveiros et al., 2020; Pereira et al., 2022; Viveiros, unpublished results); ii) directly sampled fumaroles from other localities in Macaronesia (Pico do Fogo, Fogo island, Cape Verde archipelago, Aiuppa et al., 2020; Teide, Tenerife, Canary islands, Melián et al., 2012). The Caldeira Velha fumarolic plumes exhibit the most CO_2-rich and S_T-poor compositions, well beyond the compositional field of the same fumaroles that immediately source them (small red-filled diamonds), indicating processing (H_2O condensation and sulphur scrubbing) in the soil/thermal water pool shortly prior/during surface emission. For reference, the compositional field of high-temperature magmatic gases globally is also shown (data from Aiuppa and Moussallam, 2023). (For interpretation of the references to color in this figure legend, the reader is referred to the Web version of this article.)

degassing (Fischer et al., 2019; Werner et al., 2019), our results suggest that weak hydrothermal manifestations (boiling pools and steaming grounds, including their adjacent boiling temperature fumaroles) can rival, in terms of CO_2 output, the far more spectacular crater plume emissions. This relatively large CO_2 flux is a direct consequence of the CO_2-rich nature of the gas emitted (Fig. 5) and hence does not extend to other gases. For example, H_2S and H_2 are present at minor/trace levels in these manifestations (Figs. 4–5). If we therefore combine the inferred CO_2 flux with the measured H_2S/CO_2 H_2/CO_2 ratios, we obtain H_2S and H_2 fluxes of only ~0.04 and 0.008 tons/day (Table 1). These are trivial levels compared to those sustained by crater plume degassing at the strongest volcanic gas point sources on Earth, for which a cumulative output of ~3600 and ~600 tons/day (for respectively H_2S and H_2) has recently been estimated (Aiuppa and Moussallam, 2023).

Our results here bring some novel pieces of information to our understanding of CO_2 emission budgets at both local and global scale. At the local scale, e.g., in the specific case of Fogo volcano, our observations contribute to an improved assessment of the total volcanic CO_2 output from the Caldeiras da Ribeira Grande hydrothermal zone. Previous work (Viveiros et al., 2023 and references cited therein) has reported an enlargement of the area of diffuse hydrothermal degassing at Caldeiras da Ribeira Grande since 2010. From the results of a soil CO_2 flux survey, Viveiros et al. (2023) identified in the area a diffuse degassing structure (DDS) roughly stretching in a NW-SE direction, consistent with a primary tectonic/structural control on deep gas ascent and surface release. By interpolation, the total diffuse CO_2 flux from this DDS was estimated at ~40 tons/day. However, from a comparison between measured CO_2 concentrations in air (at 0.3–1.5 m height above ground) and model results (the output of a CO_2 dispersion model), Viveiros et al. (2023) also claimed for the existence of an extra CO_2 contribution (in addition to soil degassing), which they identified in fumarolic activity. In particular, in order to match the observed pattern of air CO_2 concentrations, the authors estimated a necessary extra CO_2 flux from fumarolic activity of ~174 tons/day. Our observations here contribute to the first - although indirect - experimental quantification of the fumarolic CO_2 flux Caldeiras da Ribeira Grande, which we assess at ~118 tons/day (Table 1). This is roughly half of the total fumarolic CO_2 flux from Fogo volcano (232 ± 140 tons/day; Table 1). Importantly, our quantified ~118 tons/day flux overlaps within uncertainty (~30 %) with the fumarolic flux estimated by Viveiros et al. (2023) based on physical modelling. Our results therefore confirm that, in the specific case of Caldeiras da Ribeira Grande, fumarolic activity sustained by steaming grounds/pools/fumaroles is the primary form of CO_2 degassing, being a factor ~3 more important the diffuse CO_2 output.

Extrapolation/exportation of our Fogo results to other volcanic systems is not simple and straightforward. For example, while we find fumarolic activity prevails over diffuse degassing at Fogo, the opposite has been observed elsewhere (e.g., at Campi Flegrei, Aiuppa et al., 2013; Cardellini et al., 2017). Without additional observations at other systems, it is therefore impossible to constrain whether the relatively high fumarolic CO_2 flux determined at Fogo is unique to this system, or rather common to many others. Fischer et al. (2019) compiled a list of 278 volcanoes globally categorized as "hydrothermal" in view of the existence (inferred from analysis of GVP database, observations, reports, and photogrammetry) of hydrothermal manifestations of various kinds (steaming grounds, boiling pools, mild fumaroles). From statistical analysis, they inferred the characteristic CO_2 flux from these hydrothermal volcanoes to be 0.013 Tg/yr (with confidence intervals of 5 % and 95 % of 0.009 and 0.19 Tg/yr), which is equivalent to a daily output of 36 tons (range, 25–52 tons/day). This is a factor >6 lower than the Fogo volcano fumarolic flux inferred here. We notice that Fischer et al. (2019) based their calculations on a subset of 45 volcanoes in hydrothermal stage of activity, 38 of which having co-determined CO_2 and SO_2 fluxes. The frequent occurrence of SO_2 in the hydrothermal emissions catalogued by Fischer et al. (2019) implies these refer to a distinct category of emission forms (that of relatively hot, SO_2-rich crater fumaroles) than those studied here - boiling pools and steaming grounds on the outer volcano slope. It is therefore well possible that this latter subtle emission form, which is likely to be relatively common in the peripheries/flanks of many active and dormant volcanoes, has completely escaped cataloguing in previous volcanic CO_2 emission inventories so far (Burton et al., 2013; Werner et al., 2019; Fischer et al., 2019; Fischer and Aiuppa, 2020). If extrapolated to all 278 hydrothermal volcanoes, the Fogo flux (232 tons/day) would imply a cumulative global CO_2 flux from hydrothermal degassing of ~65,000 tons/day (or ~24 Tg/yr), emitted via steaming grounds and boiling pools (and the mild fumaroles surrounding them). For comparison, crater fumaroles and plumes from subaerial volcanoes globally are estimated to emit ~53–88 Tg/yr CO_2 (Werner et al., 2019; Fischer et al., 2019; Fischer and Aiuppa, 2020).

Our calculations here should only be viewed as illustrative and qualitative. As noted above, it is unrealistic that one system alone can be assumed as representative of global volcano behavior. Still, in addition to claiming for the need of further measurements at other volcanoes, our results suggest that hydrothermal degassing may ultimately account for a non-trivial fraction of the global volcanic CO_2 budget.

5. Conclusions

We have characterized the CO_2 emission budget from boiling pools, steaming grounds and adjacent small hydrothermal fumaroles along the outer flanks of the Fogo volcano on São Miguel island. Our results suggest that such hydrothermal manifestations, although very modest in size, still release CO_2 at levels of a few hundred tons per day, e.g., at the same rate as a medium-sized arc volcano through its crater plume. Our results indicate that hydrothermal fumaroles, boiling pools, and steaming grounds emit ~232 ± 140 tons/day of CO_2. Comparison between the Caldeiras da Ribeira Grande fumarolic flux (~118 tons/day) and the corresponding soil diffuse degassing flux (~40 tons/day) suggest that fumaroles are the main gas emission form in the area. Data at other volcanoes are needed to assess the potential global-scale CO_2 contribution from this previously overlooked hydrothermal emission category.

CRediT authorship contribution statement

Alessandro Aiuppa: Writing – original draft, Project administration, Methodology, Investigation, Funding acquisition, Formal analysis, Data curation, Conceptualization. **Fátima Viveiros:** Writing – original draft, Visualization, Project administration, Methodology, Investigation, Funding acquisition, Formal analysis, Data curation, Conceptualization. **António Cordeiro:** Methodology, Investigation, Formal analysis.

Funding

This research was funded by the MAGAT project (FCT funding, Ref. CIRCNA/OCT/2016/2019), whose PI was Vittorio Zanon. A.A. acknowledge funding from the RETURN Extended Partnership funded by the European Union Next-GenerationEU (National Recovery and Resilience Plan – NRRP, Mission 4, Component 2, Investment 1.3 – D.D. 1243 August 2, 2022, PE0000005).

Declaration of competing interest

The authors declare the following financial interests/personal relationships which may be considered as potential competing interests: Alessandro Aiuppa reports financial support was provided by European Union. Fatima Viveiros reports financial support was provided by Fundação para a Ciência e a Tecnologia. If there are other authors, they declare that they have no known competing financial interests or personal relationships that could have appeared to influence the work reported in this paper.

Acknowledgments

We wish to thank Mathilde Coron and Bruno Medeiros for support during fieldwork, as well as Hadi Cruz for reviewing the English. The manuscript benefited from constructive comments and suggestions from the Associate Editor Dr. JoAnn Holloway, Dr Peter Kelly, and one anonymous reviewer.

Appendix A. Supplementary data

Supplementary data to this article can be found online at https://doi.org/10.1016/j.apgeochem.2025.106516.

Data availability

Data will be made available on request.

References

Aiuppa, A., Moussallam, Y., 2023. Hydrogen and hydrogen sulphide in volcanic gases: abundance, processes, and atmospheric fluxes. C. R. Geosci. 356, 1–24. https://doi.org/10.5802/crgeos.235.

Aiuppa, A., Tamburello, G., Di Napoli, R., Cardellini, C., Chiodini, G., Giudice, G., Grassa, F., Pedone, M., 2013. First observations of the fumarolic gas output from a restless caldera: implications for the current period of unrest (2005-2013) at Campi Flegrei. Geochem. Geophys. Geosys. 14, 4153–4169.

Aiuppa, A., Fischer, T.P., Plank, T., Robidoux, P., Di Napoli, R., 2017. Along-arc, inter-arc and arc-to-arc variations in volcanic gas CO_2/S_T ratios reveal dual source of carbon in arc volcanism. Earth Sci. Rev. 168, 24–47.

Aiuppa, A., Fischer, T.P., Plank, T., Bani, P., 2019. CO2 flux emissions from the earth's Most actively degassing volcanoes, 2005–2015. Sci. Rep. 9, 5442. https://doi.org/10.1038/s41598-019-41901-y.

Aiuppa, A., Bitetto, M., Rizzo, A.L., Viveiros, F., Allard, P., Frezzotti, M.L., Valenti, V., Zanon, V., 2020. The fumarolic CO_2 output from Pico do Fogo volcano (Cape Verde). Ital. J. Geosci. 39 (3), 325–340. https://doi.org/10.3301/IJG.2020.03.

Aiuppa, A., Bitetto, M., Calabrese, S., et al., 2022. Mafic magma feeds degassing unrest at Vulcano Island, Italy. Commun. Earth Environ. 3, 255. https://doi.org/10.1038/s43247-022-00589-1.

Andrade, C., Cruz, J.V., Viveiros, F., Coutinho, R., 2020. CO2 emissions from Fogo intracaldera volcanic lakes (São Miguel Island, Açores): a tool for volcanic monitoring. J. Volcanol. Geoth. Res. 400, 106915. https://doi.org/10.1016/j.jvolgeores.2020.106915.

Burton, M.R., Sawyer, G.M., Granieri, D., 2013. Deep carbon emissions from volcanoes. Rev. Mineral. Geochem.: Carbon Earth 75, 323–355.

Buck, A.L., 1981. New equations for computing vapor pressure and enhancement factor. J. Appl. Meteorol. 20 (12), 1527–1532.

Caliro, S., Viveiros, F., Chiodini, G., Ferreira, T., 2015. Gas geochemistry of hydrothermal fluids of the S. Miguel and Terceira Islands, Azores. Geochem. Cosmochim. Acta 168, 43–57.

Cardellini, C., Chiodini, G., Frondini, F., et al., 2017. Monitoring diffuse volcanic degassing during volcanic unrests: the case of Campi Flegrei (Italy). Sci. Rep. 7, 6757. https://doi.org/10.1038/s41598-017-06941-2.

Carvalho, M.R., Forjaz, V.H., Almeida, C., 2006. Chemical composition of deep hydrothermal fluids in the Ribeira Grande geothermal field (São Miguel, Azores). J. Volcanol. Geoth. Res. 156, 116–134.

Chiodini, G., Marini, L., 1998. Hydrothermal gas equilibria; the H2O–H2 –CO2 –CO–CH4 system. Geochem. Cosmochim. Acta 62 (15), 2673–2687.

D'Araújo, J., Sigmundsson, F., Ferreira, T., Okada, J., Lorenzo, M., Silva, R., Carmo, R., Gaspar, J.L., 2022. - multiple inflation and deflation events from 2004 to 2016 at Fogo (Água de Pau) volcano, São Miguel, Azores. J. Volcanol. Geoth. Res. 432, 107694. https://doi.org/10.1016/j.jvolgeores.2022.107694.

Deutsch, C.V., Journel, A.G., 1998. GSLIB: geostatistical software library and user's guide. In: Appl. Geostat. Ser., vol. 369. Oxford Univ. Press, N. Y.

Ferreira, T., Oskarsson, N., 1999. Chemistry and isotopic composition of fumarole discharges of Furnas caldera. J. Volcanol. Geoth. Res. 92, 169–179.

Fischer, T.P., Arellano, S., Carn, S., et al., 2019. The emissions of CO_2 and other volatiles from the world's subaerial volcanoes. Sci. Rep. 9, 18716. https://doi.org/10.1038/s41598-019-54682-1.

Fischer, T.P., Aiuppa, A., 2020. AGU Centennial grand challenge: volcanoes and deep carbon global CO2 emissions from subaerial volcanism-recent progress and future challenges. Geochem. Geophys. Geosyst. 21, e2019GC008690. https://doi.org/10.1029/2019GC008690.

Gerlach, T.M., 1991. Present-day CO_2 emissions from volcanoes. Eos Trans. Am. Geophys. Union 72, 249–255.

Global Volcanism Program, 2024. [database] volcanoes of the world (v. 5.2.7; 21 Feb 2025). Distributed by Smithsonian Institution, compiled by Venzke, E. https://doi.org/10.5479/si.GVP.VOTW5-2024.5.2.

James, M.R., Carr, B.B., D'Arcy, F., Diefenbach, A.K., Dietterich, H.R., Fornaciai, A., Lev, E., Liu, E.J., Pieri, D.C., Rodgers, M., Smets, B., Terada, A., von Aulock, F.W., Walter, T.R., Wood, K.T., Zorn, E.U., 2020. Volcanological applications of unoccupied aircraft systems (UAS): developments, strategies, and future challenges. Volcanica 3 (1), 64–114. https://doi.org/10.30909/vol.03.01.67114.

Matias, D., Antlauf, M., Viveiros, F., Moreno, L., Silva, C., Oliveira, S., 2024. Monitoring hydrothermal fumaroles in the Azores archipelago - applications and sources of analytical uncertainties. J. Volcanol. Geoth. Res. 450, 108076. https://doi.org/10.1016/j.jvolgeores.2024.108076.

Melián, G., Tassi, F., Pérez, N., Hernández, P., Sortino, F., Vaselli, O., Padrón, E., Nolasco, D., Barrancos, J., Padilla, G., Rodríguez, F., Dionis, S., Calvo, D., Notsu, K., Sumino, H., 2012. A magmatic source for fumaroles and diffuse degassing from the summit crater of Teide Volcano (Tenerife, Canary Islands): a geochemical evidence for the 2004-2005 seismic-volcanic crisis. Bull. Volcanol. 74 (6), 1465–1483. https://doi.org/10.1007/s00445-012-0613-1.

Moore, R.B., 1990. Volcanic geology and eruption frequency, São Miguel, Azores. Bull. Volcanol. 52, 602–614.

Oppenheimer, C., Scaillet, B., Martin, R.S., 2011. Sulfur degassing from volcanoes: source conditions, surveillance, plume chemistry and impacts. Rev. Mineral. Geochem. 73, 363–421.

Oppenheimer, C., Fischer, T.P., Scaillet, B., 2014. Volcanic degassing. In: Holland, H.D., Turekian, K.K. (Eds.), Treatise on Geochemistry, the Crust, second ed. Elsevier, pp. 111–179.

Pedone, M., Viveiros, F., Aiuppa, A., Giudice, G., Grassa, F., Gagliano, A.L., Francofonte, V., Ferreira, T., 2015. Total (fumarolic and diffuse soil) CO2 output from Furnas volcano. Earth Planets Space 67 (1). https://doi.org/10.1186/s40623-015-0345-5 art. no. 174.

Pereira, M.L., Matias, D., Viveiros, F., Moreno, L., Silva, C., Zanon, V., Uchˆoa, J., 2022. The contribution of hydrothermal mineral alteration analysis and gas geothermometry for understanding high-temperature geothermal fields - the case of Ribeira Grande geothermal field, Azores. Geothermics 105, 102519. https://doi.org/10.1016/j.geothermics.2022.102519.

Pérez, N.M., Hernández, P.A., Padilla, G., Nolasco, D., Barrancos, J., Melián, G., Padrón, E., Dionis, S., Calvo, D., Rodríguez, F., Notsu, K., Mori, T., Kusakabe, M., Arpa, M.C., Reniva, P., Ibarra, M., 2011. Global CO_2 emission from volcanic lakes. Geol. 39, 235–238.

Pimentel, J., 2024. Contributo para o estudo das emanações gasosas permanentes de CO2 e 222Rn no flanco sul do Vulcão do Fogo (São Miguel, Açores). Master Thesis in Volcanology and Risks Assessment, University of the Azores, p. 171 (in Portuguese).

Silva, R., Havskov, J., Bean, C., Wallenstein, N., 2012. Seismic swarms, fault plane solutions and stress tensors for São Miguel Island central region (Azores). J. Seismol. https://doi.org/10.1007/s10950-012-9275-x.

Silva, R., Carmo, R., Marques, R., 2020. Characterization of the Tectonic Origins of Historical and Modern Seismic Events and Their Societal Impact on the Azores Archipelago, vol. 501. Geological Society, London, Special Publications, Portugal. https://doi.org/10.1144/SP501-2019-106.

Syracuse, E.M., Abers, G.A., 2006. Global compilation of variations in slab depth beneath arc volcanoes and implications. Geochem. Geophys. Geosyst. 1219 (7). https://doi.org/10.1029/2005GC001045.

Sleep, N.H., Zahnle, K., 2001. Carbon dioxide cycling and implications for climate. J. Geophys. Res. 106, 1373–1399.

Steinthorsdottir, M., Montañez, I.P., Royer, D.L., Mills, B.J.W., Hönisch, B., 2025. Phanerozoic atmospheric CO_2 reconstructed with proxies and models: current understanding and future directions. Geochem. Treatise 5, 467–492. https://doi.org/10.1016/B978-0-323-99762-1.00074-7.

Stix, J., de Moor, J.M., 2018. Understanding and forecasting phreatic eruptions driven by magmatic degassing. Earth Planets Space 70, 83. https://doi.org/10.1186/s40623-018-0855-z.

Stix, J., Nadeau, P., Aguilera, F., Burton, M., Chiodi, A., 2025. Volcanic degassing. In: Bonadonna, C., Caricchi, L., Clarke, A., Cole, P., Lindsay, J., Lowenstern, J., Robertson, R., Villegas, M.L. (Eds.), Encyclopedia of Volcanoes, third ed. Part 3, Chapter 2.8.

Uchôa, J., Viveiros, F., Tiengo, R., Gil, A., 2023. Detection of Geothermal Anomalies in Hydrothermal Systems Using ASTER Data: the Caldeiras da Ribeira Grande Case Study (Azores, Portugal). Sensors 23, 2258. https://doi.org/10.3390/s23042258.

Viveiros, F., Ferreira, T., Cabral Vieira, J., Silva, C., Gaspar, J.L., 2008. Environmental influences on soil CO_2 degassing at Furnas and Fogo volcanoes (São Miguel Island, Azores archipelago). J. Volcanol. Geoth. Res. 177, 883–893. https://doi.org/10.1016/j.jvolgeores.2008.07.005.

Viveiros, F., Cardellini, C., Ferreira, T., Caliro, S., Chiodini, G., Silva, C., 2010. Soil CO_2 emissions at Furnas volcano, São Miguel Island, Azores archipelago: volcano monitoring perspectives, geomorphologic studies, and land use planning application. J. Geophys. Res. 115, B12208. https://doi.org/10.1029/2010JB007555.

Viveiros, F., Ferreira, T., Silva, C., Vieira, J.C., Gaspar, J.L., Virgili, G., Amaral, P., 2015a. Permanent monitoring of soil CO_2 degassing at Furnas and Fogo volcanoes (São Miguel Island, Azores). Geol. Soc. Lond. Mem. 44, 271–288. https://doi.org/10.1144/M44.20.

Viveiros, F., Gaspar, J.L., Ferreira, T., Silva, C., Marcos, M., Hipólito, A., 2015b. Mapping of soil CO_2 diffuse degassing at São Miguel Island and its public health implications. Geol. Soc. Lond. Mem. 44, 185–195. https://doi.org/10.1144/M44.14.

Viveiros, F., Chiodini, G., Cardellini, C., Caliro, S., Zanon, V., Silva, C., Rizzo, A.L., Hipólito, A., Moreno, L., 2020. Deep CO_2 emitted at Furnas do enxofre geothermal area (Terceira Island, Azores archipelago). An approach for determining CO_2 sources and total emissions using carbon isotopic data. J. Volcanol. Geoth. Res. 401, 106968. https://doi.org/10.1016/j.jvolgeores.2020.106968.

Viveiros, F., Baldoni, E., Massaro, S., Stocchi, M., Costa, A., Caliro, S., Chiodini, G., Andrade, C., 2023. Quantification of CO2 degassing and atmospheric dispersion at Caldeiras da Ribeira Grande (São Miguel Island, Azores). J. Volcanol. Geoth. Res. 438, 107807. https://doi.org/10.1016/j.jvolgeores.2023.107807.

Wallace, P.J., Plank, T., Edmonds, M., Hauri, E.H., 2015. Volatiles in Magmas. In: Sigurdsson, H. (Ed.), The Encyclopedia of Volcanoes, second ed. Academic Press, pp. 163–183.

Wallenstein, N., Duncan, A., Guest, J.E., Almeida, M.H., 2015. Eruptive history of Fogo Volcano, Sao Miguel, Azores in. In: Gaspar, J.L., Guest, J.E., Duncan, A.M., Barriga, F.J.A.S., Chester, D.K. (Eds.), Volcanic Geology of Sãoo Miguel Island (Azores Archipelago), vol. 44. Geological Society, London, Memoirs, pp. 105–123. https://doi.org/10.1144/M44.8, 2015, Published by The Geological Society of London.

Walker, G.P.L., Croasdale, R., 1971. Two plinian-type eruptions in the Azores. J. Geol. Soc. 127, 17–55. https://doi.org/10.1144/gsjgs.127.1.0017. London.

Werner, C., Evans, W.C., Poland, M., Tucker, D.S., Doukas, M.P., 2009. Long-term changes in quiescent degassing at Mount Baker Volcano, Washington, USA; evidence for a stalled intrusion in 1975 and connection to a deep magma source. J. Volcanol. Geoth. Res. 186, 379–386.

Werner, C., et al., 2019. Carbon dioxide emissions from subaerial volcanic regions. In: Orcutt, Beth N., Daniel, Isabelle, Dasgupta, Rajdeep (Eds.), Deep Carbon: past to Present. Cambridge University Press. https://doi.org/10.1017/9781108677950.

Williams, S.N., Schaefer, S.J., Marta Lucia Calvache, V., Lopez, D., 1992. Global carbon dioxide emission to the atmosphere by volcanoes. Geochem. Cosmochim. Acta 56, 1765–1770.

Wong, K., Mason, E., Brune, S., East, M., Edmonds, M., Zahirovic, S., 2019. Deep carbon cycling over the past 200 million years: a review of fluxes in different tectonic settings. Front. Earth Sci. 7. https://doi.org/10.3389/feart.2019.00263 art. no. 263.